






Article

Towards High CO₂ Conversions Using Cu/Zn Catalysts Supported on Aluminum Fumarate Metal-Organic Framework for Methanol Synthesis

Zama G. Duma^{1,2,*}, John Moma², Henrietta W. Langmi³, Benoit Louis⁴, Ksenia Parkhomenko⁴
and Nicholas M. Musyoka^{1,*}

- ¹ Centre for Nanostructures and Advanced Materials (CeNAM), Chemicals Cluster, Council for Scientific and Industrial Research (CSIR), Meiring Naudé Road, Brummeria, Pretoria 0184, South Africa
- ² Molecular Sciences Institute, School of Chemistry, University of the Witwatersrand, Private Bag, Johannesburg 2050, South Africa
- ³ Department of Chemistry, University of Pretoria, Private Bag X20, Hatfield 0028, South Africa
- ⁴ Energy and Fuels for a Sustainable Environment Team, Institut de Chimie et Procédés pour l'Energie, l'Environnement et la Santé, UMR 7515 CNRS—ECPM, Université de Strasbourg, 25 rue Becquerel, CEDEX 2, 67087 Strasbourg, France
- * Correspondence: zduma@csir.co.za (Z.G.D.); nmusyoka@csir.co.za (N.M.M.); Tel.: +27-12-841-4806 (N.M.M.)

Abstract: Green methanol is a viable alternative for the storage of hydrogen and may be produced from captured anthropogenic sources of carbon dioxide. The latter was hydrogenated over Cu-ZnO catalysts supported on an aluminum fumarate metal-organic framework (AlFum MOF). The catalysts, prepared via slurry phase impregnation, were assessed for thermocatalytic hydrogenation of CO₂ to methanol. PXRD, FTIR, and S_{BET} exhibited a decrease in crystallinity of the AlFum MOF support after impregnation with Cu-Zn active sites. SEM, SEM-EDS, and TEM revealed that the morphology of the support is preserved after metal loading, where H₂-TPR confirmed the presence of active sites for hydrogen uptake. The catalysts exhibited good activity, with a doubling in Cu and Zn loading over the AlFum MOF, resulting in a 4-fold increase in CO₂ conversions from 10.8% to 45.6% and an increase in methanol productivity from 34.4 to 56.5 g_{MeOH}/Kg_{cat}/h. The catalysts exhibited comparatively high CO selectivity and high yields of H₂O, thereby favoring the reverse water-gas shift reaction. The selectivity of the catalysts towards methanol was found to be 12.9% and 6.9%. The performance of the catalyst supported on AlFum MOF further highlights the potential use of MOFs as supports in the heterogeneous thermocatalytic conversion of CO₂ to value-added products.

Keywords: CO₂ hydrogenation; green methanol; reverse water-gas shift reaction; metal-organic frameworks; catalysis



Citation: Duma, Z.G.; Moma, J.; Langmi, H.W.; Louis, B.; Parkhomenko, K.; Musyoka, N.M. Towards High CO₂ Conversions Using Cu/Zn Catalysts Supported on Aluminum Fumarate Metal-Organic Framework for Methanol Synthesis. *Catalysts* **2022**, *12*, 1104. <https://doi.org/10.3390/catal12101104>

Academic Editor: Francis Verpoort

Received: 30 August 2022

Accepted: 19 September 2022

Published: 24 September 2022

Publisher's Note: MDPI stays neutral with regard to jurisdictional claims in published maps and institutional affiliations.



Copyright: © 2022 by the authors. Licensee MDPI, Basel, Switzerland. This article is an open access article distributed under the terms and conditions of the Creative Commons Attribution (CC BY) license (<https://creativecommons.org/licenses/by/4.0/>).

1. Introduction

It is evident that the continuous increase in anthropogenic CO₂ levels in the atmosphere has resulted in global warming, which leads to higher average temperatures on Earth and an increase in the acidity of oceans [1–3]. As such, driven by the large-scale combustion of carbonaceous fossil fuel sources such as coal, natural gas, and oil, CO₂ concentrations have increased by 20% in the past four decades [4]. Therefore, to abate climate change, the mitigation of CO₂ emissions is required via capture, storage, and utilization. The latter includes the chemical transformation of CO₂ to value-added chemicals such as, inter alia, methanol, dimethyl ether, organic acids, higher alcohols, and hydrocarbons [4,5]. The valorized products have a myriad of applications as chemical feedstocks and in direct usage, and in the case of methanol, as fuel sources in internal combustion engines, which makes it an ideal energy carrier [6,7].

The chemical conversion of CO₂ to methanol is predominantly carried out over ternary co-precipitated Cu/ZnO/Al₂O₃ catalysts, which are typically used for methanol production from synthesis gas (CO, CO₂, H₂), at industrial conditions of 210–300 °C and 50–80 bar [8–11]. However, the deactivation of the catalysts driven by thermal sintering of the Cu particles, phase segregation of ZnO and Al₂O₃ from Cu active sites, and decreased dispersion result in poor performance concerning the selectivity to methanol, thereby facilitating CO production [12–14]. Furthermore, zinc has been reported to react with the Al₂O₃ promoter to form zinc aluminates, which further deactivates the catalyst [14]. As such, the preparation of supported catalysts that favor good Cu dispersion, high activity toward CO₂ hydrogenation, and methanol selectivity may prevent the aforementioned catalyst deactivation mechanisms [15]. Therefore, the usage of metal-organic frameworks (MOFs), which are materials with exceptional crystallinity, high surface area, and good porosity with a large surface area as supports for Cu-based catalysts promises to circumvent the poor performance inherent to ternary, co-precipitated Cu-based catalysts [16,17].

The application of MOFs, characterized by metal-ion clusters coordinated to multi-dentate ligands, as catalyst supports has been reported to increase methanol selectivity and turnover frequency [18,19]. Therefore, the ability of MOFs as supports that have high metallic active phase dispersion makes them attractive in heterogeneous catalysis [20]. In this study, we present, for the first time according to our knowledge, the loading of Cu-ZnO on aluminum fumarate MOF (AlFum MOF) for the thermocatalytic hydrogenation of CO₂ to methanol.

2. Results

2.1. Characterization

2.1.1. Powder X-ray Diffraction (PXRD) and Fourier Transform Infrared Spectroscopy (FTIR)

The PXRD patterns of the catalysts supported on AlFum MOF are shown in Figure 1a. The 7Cu/3ZnO/AlFum MOF catalyst exhibits a diffraction pattern typical of AlFum MOF, with characteristic peaks at $2\theta = 10.2^\circ$, 14.9° , 21.1° , 31.8° and 42.7° , with no Cu or Zn peaks observed, which may be due to low metal loading, and good dispersion [16,21]. Figure 1a also shows the diffraction pattern of the pristine AlFum MOF whereas Figure 1b, zooms into the $30^\circ < 2\theta < 40^\circ$ region of Cu/ZnO/AlFum MOF catalysts. In comparison to 7Cu/3ZnO/AlFum MOF, 15Cu/6.4ZnO/AlFum MOF has double the loading of Cu and Zn and, as a result, a CuO peak at $2\theta = 38.7^\circ$ can be observed [7,22]. Furthermore, it can be seen that the crystallinity of the AlFum MOF in the supported catalysts decreases, which may be due to the high thermal treatment temperature of 350 °C under a constant flow of argon during thermal activation.

The FTIR spectra of the pristine AlFum MOF and Cu/ZnO/AlFum MOF catalysts are shown in Figure 1c–e. The broad peak at $3400\text{--}3600\text{ cm}^{-1}$ is ascribed to O-H vibrations from physisorbed or intercrystalline water and/or absorbed moisture [23–25]. The symmetric and asymmetric vibrations of the fumarate carboxylate group can be seen at 1403 and 1591 cm^{-1} [21,23]. Furthermore, it can be seen in the Cu/ZnO/AlFum MOF catalysts, Figure 1c,d, that after impregnation and thermal treatment, the intensity of the peaks decreases, which corroborates the decrease in crystallinity observed in the PXRD diffractograms, as shown in Figure 1a,b.

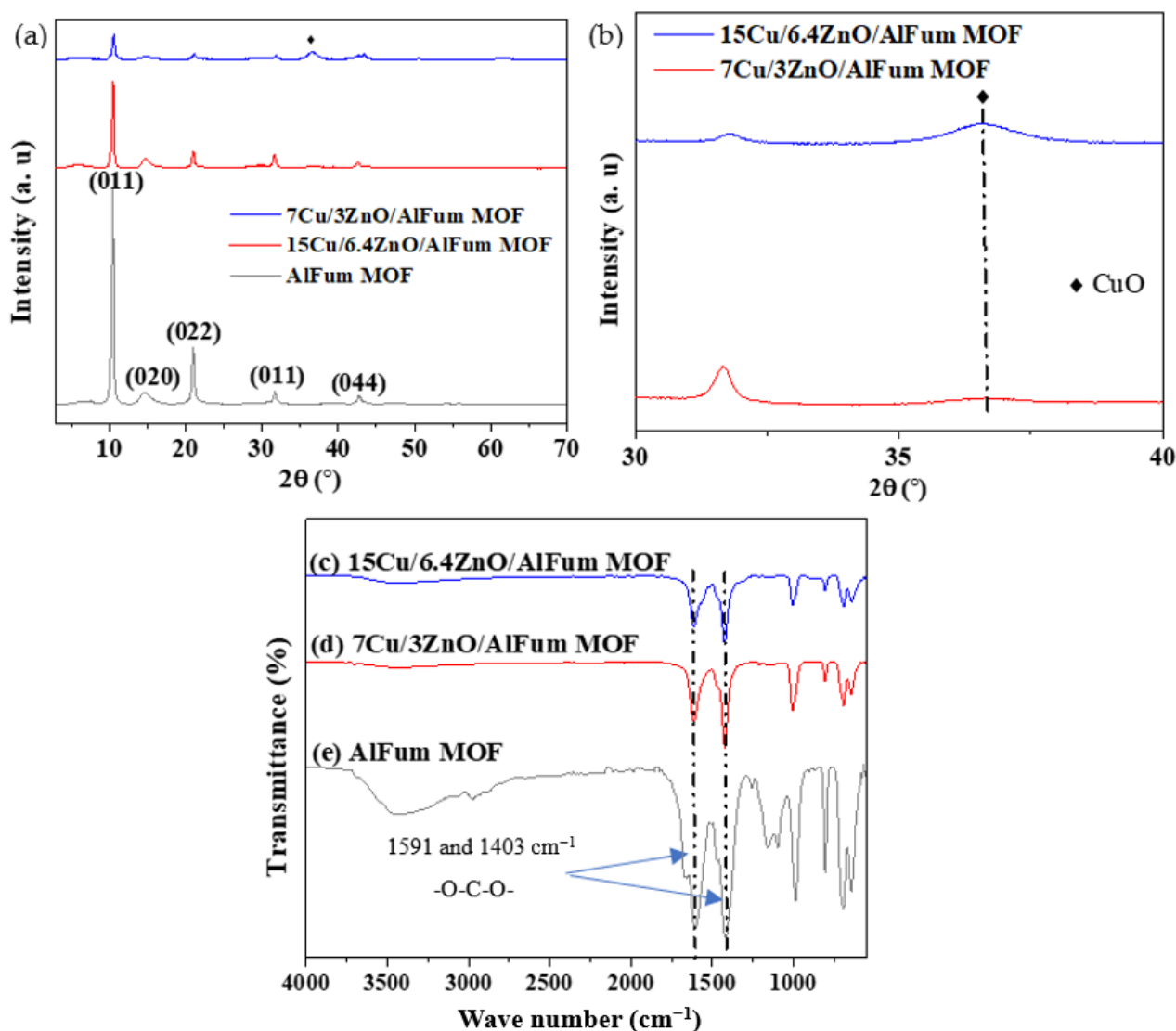


Figure 1. PXRD patterns of (a) AlFum MOF, 7Cu/3ZnO/AlFum MOF, 15Cu/6.4ZnO/AlFum MOF; (b) 7Cu/3ZnO/AlFum MOF, 15Cu/6.4ZnO/AlFum MOF at $30^\circ < 2\theta < 40^\circ$; and (c–e) FTIR spectra of AlFum MOF, 7Cu/3ZnO/AlFum MOF, and 15Cu/6.4ZnO/AlFum MOF. CuO (♦).

2.1.2. N₂ Sorption, and Elemental Loading

The pristine AlFum MOF exhibited a BET surface area (S_{BET}) of 910 m²/g, which is consistent with previously reported values [26]. The nitrogen sorption isotherms of the pristine and AlFum MOF-supported catalysts are shown in Figure 2a whereas the H-K pore volumes and NLDFT PSDs are summarized in Table 1. It can be observed that the pristine MOF and catalysts exhibit type-I sorption isotherms, which are indicative of their microporous structure [16]. In addition, the PSDs, shown in Figure 2b, show that the majority of the pores in the AlFum MOF-support and catalysts are in the micropore range, with a median pore diameter below 2 nm, as shown in Table 1 [21,23]. Furthermore, the decrease in S_{BET} observed in the impregnated MOFs to 757 and 416 m²/g is due to the loading of Cu and Zn active sites and thermal treatment [16,27]. The decrease in S_{BET} observed in both the AlFum MOF-supported catalysts is consistent with the decrease in the intensity of the PXRD and FTIR peaks in Figure 1. In addition, a decrease in the pore volume of 0.344 cm³/g in pristine AlFum MOF upon impregnation to 0.300 and 0.148 cm³/g in the 7Cu/3ZnO/AlFum MOF and 15Cu/6.4ZnO/AlFum MOF catalysts is shown in Table 1. Furthermore, SEM-EDX elemental analysis revealed a Cu loading of 11.2 wt% and 18.2 wt% compared with a theoretical composition of 7 and 15 wt% shown in parentheses.

In addition, the Zn content was 3.12 and 5.77 wt% in the Cu/ZnO/AlFum MOF and 7Cu/3ZnO/AlFum MOF catalysts, respectively. This discrepancy may be attributed to high Cu dispersion in the framework of the AlFum MOF support with regions of surface enrichment, potentially leading to higher Cu content albeit it must be noted that SEM-EDX is a semi-quantitative technique and other techniques such as inductively coupled plasma optical emission spectroscopy may provide more accurate, quantitative, elemental analysis results [28,29].

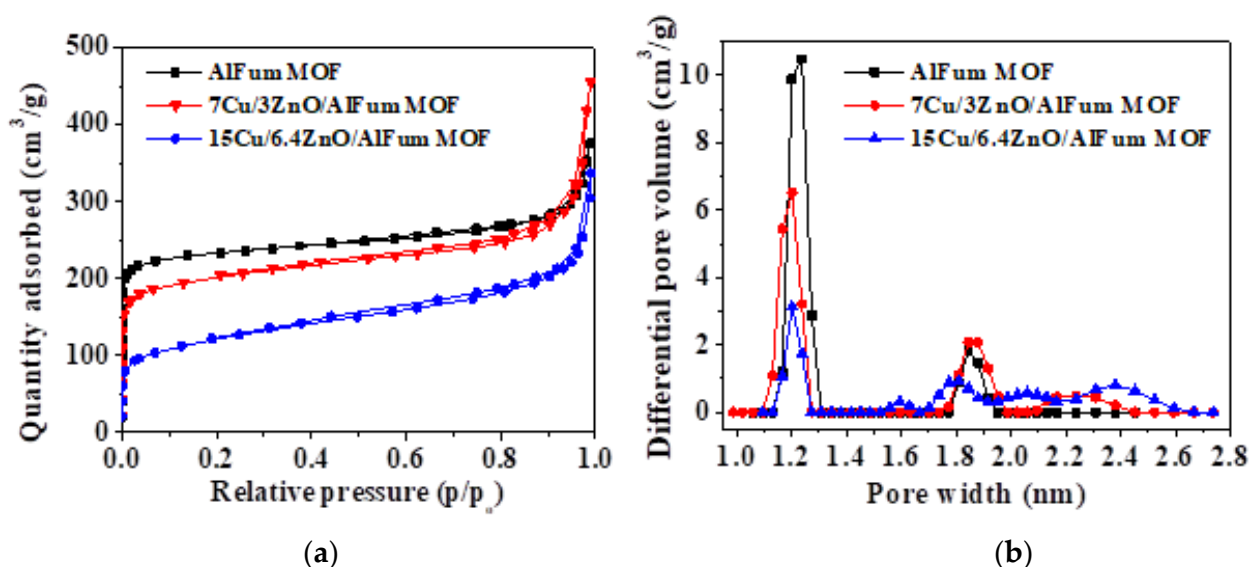


Figure 2. N₂ sorption isotherms at 77 K of: (a) AlFum MOF, 7Cu/3ZnO/AlFum MOF, 15Cu/6.4ZnO/AlFum MOF; and (b) NLDFT pore size distributions of AlFum MOF, 7Cu/6.4ZnO/AlFum MOF, and 15Cu/6.4ZnO/AlFum MOF.

Table 1. S_{BET}, pore volume, mean pore size diameter, and elemental composition of pristine AlFum MOF and Cu/ZnO/AlFum MOF catalysts.

Sample	S _{BET} (m ² /g)	Pore Volume (cm ³ /g)	d (nm)	Elemental Loading (Weight %)	
				Cu	Zn
AlFum MOF	910	0.344	1.27	-	-
7Cu/3ZnO/AlFum MOF	757	0.300	1.23	11.2 (7)	3.12 (3)
15.4Cu/6.4ZnO/AlFum MOF	416	0.148	1.30	18.2 (15)	5.77 (6.4)

2.1.3. Electron Microscopies

The morphology images obtained using SEM and TEM of the pristine AlFum MOF support and Cu/ZnO/AlFum MOF catalysts are shown in Figure 3. The AlFum MOF support particles exhibit a lozenge, quadrilateral shape characterized by the geometry of Al-octahedra coordinated by fumarate linkers [23,30]. The AlFum MOF particles exhibit some degree of agglomeration, which is consistent with literature reports [26]. The Cu/ZnO/AlFum MOF catalysts, as shown in Figure 3c–f, have a similar quadrilateral morphology to the pristine AlFum MOF prepared via the solvothermal method, as shown in Figure 3a,b [31]. Therefore, it can be seen that the morphology of the AlFum MOF support is preserved after impregnation, drying, and thermal treatment. This may be attributed to the good relative thermal stability of the support [32]. The SEM-EDX elemental maps of the 7Cu/3ZnO/AlFum MOF and 15Cu/6.4ZnO/AlFum MOF catalysts are shown in Figure 3g,h.

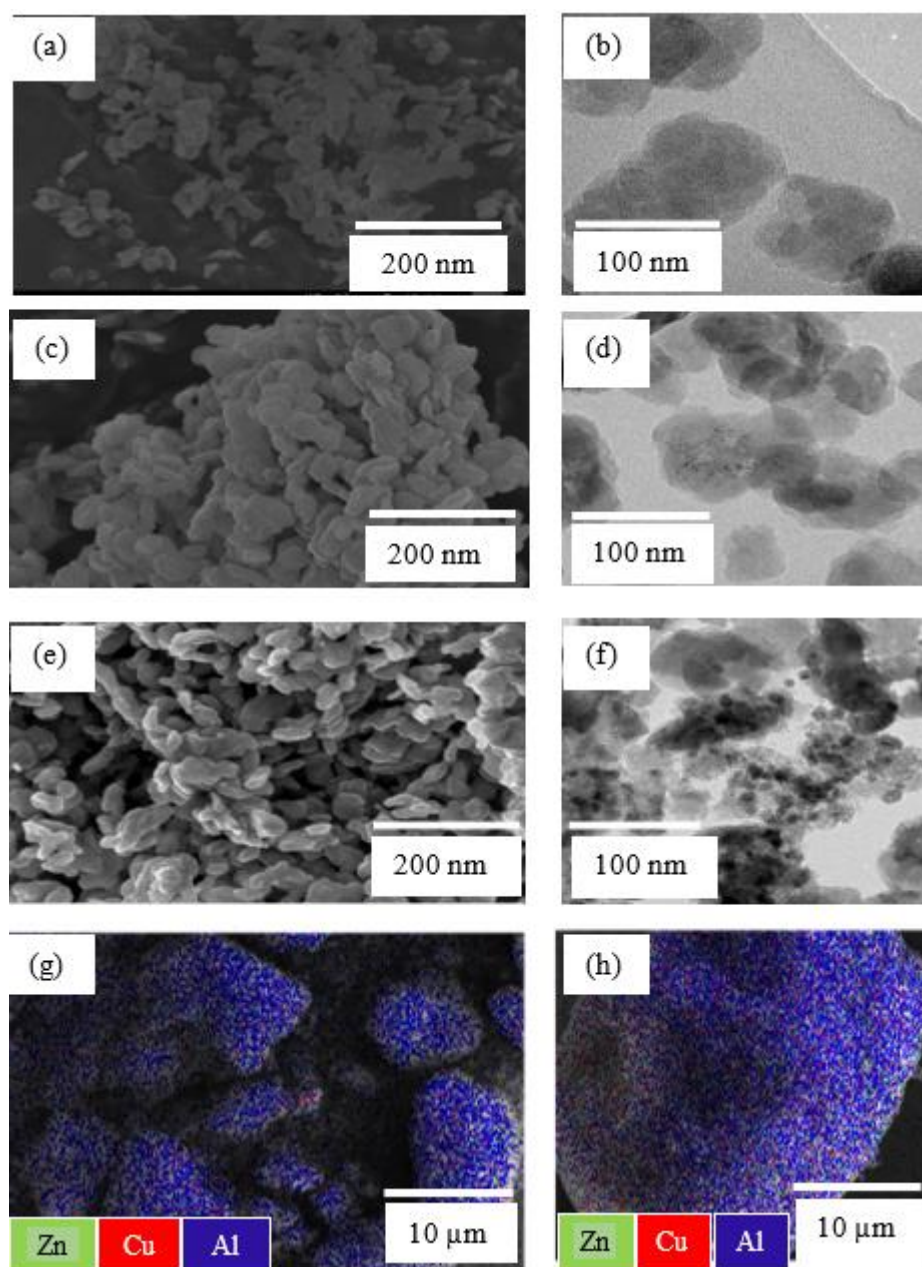


Figure 3. SEM and TEM images of: (a,b) AlFum MOF; (c,d) 7Cu/3ZnO/AlFum MOF; (e,f) 15Cu/6.4ZnO/AlFum MOF; EDX elemental maps of (g) 7Cu/3ZnO/AlFum MOF; and (h) 15Cu/6.4ZnO/AlFum MOF.

In both catalysts, a uniform, homogenous distribution of Cu and Zn is observed, which is indicative of successful impregnation. In addition, the micrographs show that in contrast to the pristine AlFum MOF support in Figure 3a,b, tiny spherical nanoparticles can be observed on the surface of the MOF support in the catalysts, which may be attributed to Cu and Zn nanoparticles, as shown in Figure 3c–f. The individual SEM-EDX elemental maps of each metal in the 7Cu/3ZnO/AlFum MOF and 15Cu/6.4ZnO/AlFum MOF catalysts are shown in Figures S1 and S2 (Supplementary Material), where the homogenous, uniform dispersion of Cu and Zn over the AlFum MOF support observed in Figure 3g,h is further corroborated.

2.1.4. Thermogravimetric Analysis (TGA) and Hydrogen-Temperature Programmed Reduction (H₂-TPR)

The TGA profiles of the pristine AlFum MOFs and Cu/ZnO/AlFum MOF catalysts are shown in Figure 4a whereas the derivative TGA plots are shown in Figures S3–S5 (Supplementary Material). The TGA profile of the pristine AlFum MOF is consistent with previously reported literature results, where the initial mass loss below 100 °C is attributed to physisorbed water, which is in accordance with the -OH bending vibration FTIR peak at 3300–3600 cm⁻¹ in FTIR, as shown in Figure 1c–e [21,24]. The weight loss peak at 172 °C is due to the removal of residual DMF solvent used during the synthesis step, as shown in Figure 4a [24]. The derivative TGA plot of the pristine AlFum MOF is shown in Figure S3 (Supplementary Material), where an additional weight loss peak at 469 °C indicates the thermal degradation of the fumarate organic linkers [21]. In addition, the TGA profiles and derivative TGA plots (Supplementary Material, Figures S3–S5) reveal that the thermal stability in the catalysts decreases after impregnation and thermal activation, where the weight loss of the fumarate organic linker temperatures shifts from 469 °C in the pristine AlFum MOF to 375 and 370 °C in the 7Cu/3ZnO/AlFum MOF and 15Cu/6.4ZnO/AlFum MOF catalysts (Supplementary Material, Figures S3–S5). The rapid weight loss indicates the decomposition of the organic linkers followed by the formation of relatively thermally stable metal oxides [21,33,34].

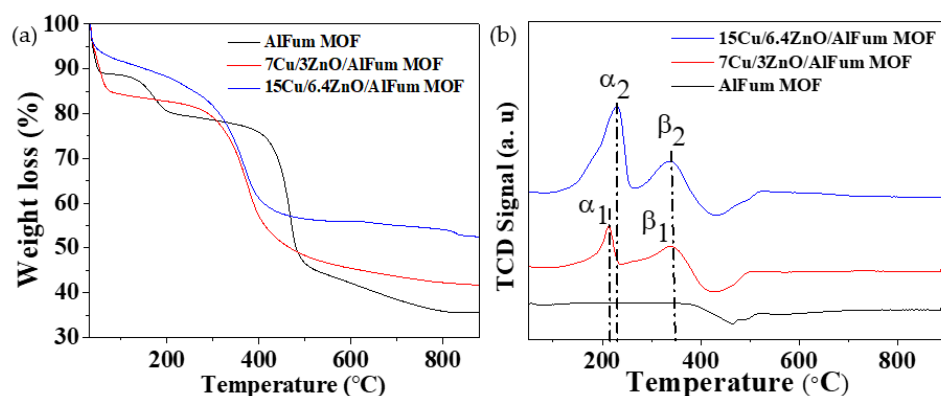


Figure 4. (a) TGA profiles of AlFum MOF, 7Cu/3ZnO/AlFum MOF, 15Cu/ZnO/6.4AlFum MOF; (b) H₂-TPR profiles of: AlFum MOF, 7Cu/3ZnO/AlFum MOF, 15Cu/6.4ZnO/AlFum MOF.

The H₂-TPR profiles of 7Cu/3ZnO/AlFum MOF and 15Cu/6.4ZnO/AlFum MOF catalysts exhibit α reduction peaks indicative of the presence of CuO at T_{max} = 213 °C (α₁) and 229 °C (α₂), as shown in Figure 4b. The β peaks at T_{max} = 339 °C (β₁) and 340 °C (β₂) indicate the presence of a second phase of CuO that formed after thermal treatment [35]. The α peaks indicate the reduction in Cu ions or CuO clusters that are in close contact with the AlFum MOF whereas the β peaks indicate the reduction in “bulk-like” CuO particles [36]. Furthermore, the α peaks indicate the reduction in finely dispersed CuO particles over the surface of the AlFum MOF support [37]. The H₂-reduction peaks further corroborate the successful loading of Cu and the formation of the desired CuO species after thermal treatment. The pristine peak of AlFum MOF did not show any reduction peaks due to the absence of Cu active sites.

2.1.5. X-ray Photoelectron Spectroscopy (XPS)

The surface oxidation states of the Cu and Zn active sites in the catalysts are shown in Figure 5. Conventionally, the peaks at 932.5 ± 0.2 and 952.3 ± 0.2 eV indicate Cu⁺ 2p_{3/2} and 2p_{1/2} oxidation states whereas the peaks at 933.7 ± 0.2 and 953.6 ± 0.2 eV are ascribed to Cu²⁺ 2p_{3/2} and 2p_{1/2}, respectively [38,39]. In addition, a satellite peak at 943.2 eV is indicative of Cu²⁺ [39]. In both catalysts, the peaks at 935 and 954 eV are indicative of the Cu²⁺ species, which is further corroborated by the satellite peak at 944 eV, respectively [40].

The XPS spectra confirm the presence of CuO in both catalysts. Figure 5b shows the spectra of Zn 2p, where the peaks at 1022 and 1046 eV indicate the presence of Zn²⁺ 2p_{3/2} and 2p_{1/2} [41].

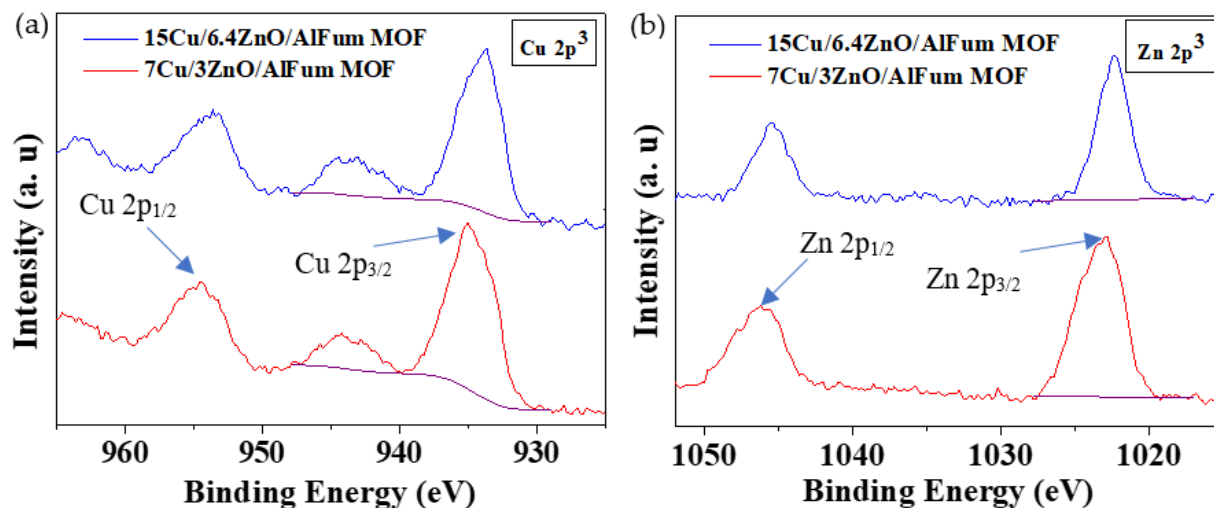
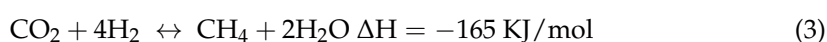
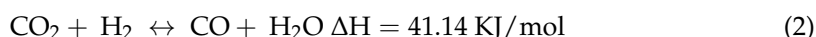
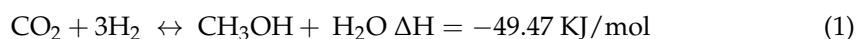


Figure 5. XPS spectra (a) Cu 2p and (b) Zn 2p of 7Cu/3ZnO/AlFum MOF and 15Cu/6.4ZnO/AlFum MOF catalysts.

2.2. Catalysts' Testing and Evaluation

Conversions, Selectivity, and Productivity

The CO₂ conversion results of all tested catalysts, including a commercial catalyst, are shown in Figure 6. The main reaction of interest is the exothermic, direct CO₂ hydrogenation to methanol shown in Equation (1). In addition to methanol, the catalysts formed CO, H₂O, and CH₄, with no other products observed. The competing, endothermic reverse water-gas shift reaction (RWGS) results in the formation of CO, where CO₂ is hydrogenated to CO and H₂O, as shown in Equation (2) [8,12,17,42,43]. In addition, CH₄ was a by-product that was formed in the reactor presumably from the Sabatier reaction, where CO₂ methanation occurs to form CH₄ and H₂O as shown in Equation (3) [44]. The 15Cu/6.4ZnO/AlFum MOF catalyst (45.6%) had the best average CO₂ conversion after 24 h onstream in comparison to the commercial catalyst (29.8%) and the 7Cu/3ZnO/AlFum MOF catalyst (10.8%), respectively. In addition, the catalysts showed relatively good stability over the 24-h testing period. In our previous studies of the thermodynamic equilibrium of the CO₂ hydrogenation reaction, it was shown that the best H₂ and CO₂ conversions and the optimal CH₃OH selectivity are obtained at low temperatures. For example, at 50 bars and 230 °C, the conversion of CO₂ could achieve 37% and 25% for H₂ conversion [45]. At high temperatures, the additional increase in CO₂ conversion up to 45% is clearly correlated with CO production with 100% selectivity. Such high conversion (45.6%) observed in the 15Cu/6.4ZnO/AlFum MOF catalyst at a lower temperature of 230 °C is phenomenal and could be correlated to the changes in the selectivity and thus extensive CO production and the presence of CH₄. The continuous increase in the slope of the CO₂ conversion for 7Cu/3ZnO/AlFum MOF catalyst could be attributed to the reconstruction of the catalytic active sites during reaction; more precisely, the formation of metallic copper nanoparticles stabilized by the concomitant structure. Due to the low copper loading in the 7Cu/3ZnO/AlFum MOF catalyst, the nanoparticles grow, and stabilization may take time:



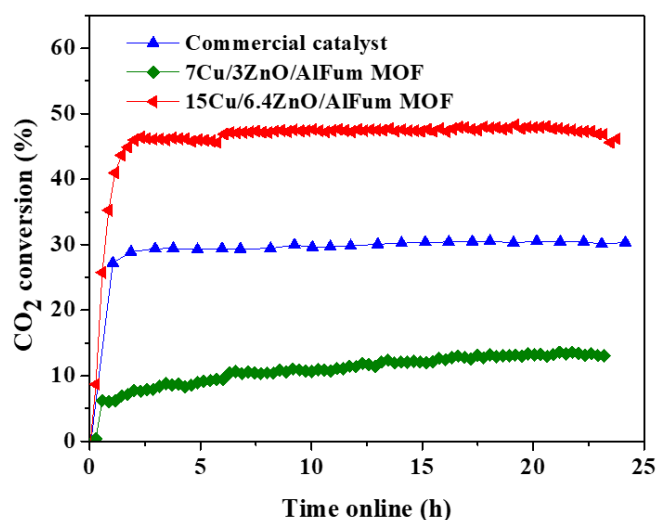


Figure 6. CO₂ conversions of the evaluated catalysts. Temperature = 230 °C; pressure = 50 bar; Q_{v,0} = 40 mL min⁻¹; gas hourly space velocity = 10,000 h⁻¹; H₂/CO₂ = 3:1.

The methanol selectivity of the catalysts was also investigated. The commercial catalyst exhibited the highest selectivity (15.0%) whereas 7Cu/3ZnO/AlFum MOF and 15Cu/6.4ZnO/AlFum MOF exhibited relatively lower methanol selectivity of 12.9% and 6.9%, as shown in Figure 7a. In addition, CO was produced by all the evaluated catalysts due to the competing RWGS reaction [46]. The evaluated catalysts' selectivity to CO was significant in all catalysts, with the highest at 88% displayed by the 15Cu/6.4ZnO/AlFum MOF catalyst followed by the 7Cu/3ZnO/AlFum MOF catalyst (85.2%) whereas the selectivity of the commercial catalyst was the lowest at 84%, as shown in Figure 7a. In addition, the catalysts produced CH₄, which is attributed to the CO₂ methanation reaction [44]. Therefore, the 15Cu/6.4ZnO/AlFum MOF and 7Cu/3ZnO/AlFum MOF catalysts had the highest selectivity to CH₄ at 5.17% and 1.82%, respectively, whereas the commercial catalyst had the lowest CH₄ selectivity at 0.93%. Furthermore, the mole product distribution, as shown in Table 2, indicates that the catalysts form a significantly larger amount of CO and H₂O, which further corroborates the high selectivity towards CO, which is attributed to the RWGS reaction. Furthermore, all the catalysts produced 48–50% of H₂O due to both the RWGS and CO₂ to methanol reaction shown in Equations (1) and (2), respectively.

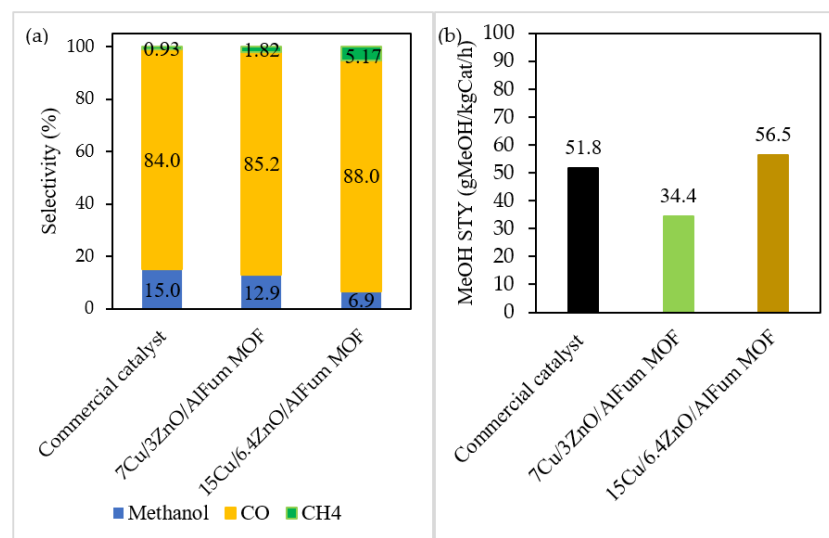


Figure 7. (a) MeOH, CO, and CH₄ selectivity and (b) MeOH space-time yield of all the tested catalysts.

Table 2. Product distribution for all the evaluated catalysts.

Catalyst	Product Distribution (mol%)			
	MeOH	CO	CH ₄	H ₂ O
Commercial	12.8	36.0	2.50	48.7
7Cu/3ZnO/AlFum MOF	6.50	42.8	0.9	49.8
15Cu/6.4ZnO/AlFum MOF	3.48	44.6	2.62	49.3

In contrast, Bonura et al. observed a methanol selectivity of 49% using copper-zinc-zirconia catalysts at 240 °C, 30 bar, and GHSV of 10,000 h⁻¹. However, the catalysts had a relatively low degree of CO₂ conversion of 16.8% compared with 15Cu/6.4ZnO/AlFum MOF catalyst (45.6%) [47]. Furthermore, An et al. also reported a comparatively high methanol selectivity of 100% albeit the CO₂ conversion was 3.3% at 250 °C, 40 bar, and GHSV of 6000 h⁻¹ [40]. Though the 15Cu/6.4ZnO/AlFum MOF catalyst showed relatively low selectivity toward methanol, it exhibited a superior degree of CO₂ conversion. As such, the dispersion of Cu and Zn active sites on AlFum MOF demonstrates the advantages of using highly crystalline, high surface area, porous materials, where 10–15% of the active sites may be loaded on the catalysts as opposed to 70% in conventional, co-precipitated catalysts. Furthermore, AlFum MOF is commercially sold by BASF as Basolite A520TM, and a water-based green synthesis procedure has been adopted for the production of green AlFum MOF at a ton-level. Therefore, the scalability of the AlFum MOF via a green, hydrothermal process makes the MOF, Basolite A520TM, a sustainable and alternative support for Cu-based catalysts to drive sustainable CO₂ capture and utilization [26,30,31,48].

The methanol space-time yield (STY) obtained over 15Cu/6.4ZnO/AlFum MOF catalyst was found to be 56.5 g_{MeOH}/kg_{cat}/h followed by the commercial catalyst at 51.8 g_{MeOH}/kg_{cat}/h, whereas 7Cu/3ZnO/AlFum MOF catalyst led to the lowest STY of 34.4 g_{MeOH}/kg_{cat}/h (Figure 7b). The methanol STY increased with an increase in the Cu loading: 11.2% (7Cu/3ZnO/AlFum MOF), 18.2% (15Cu/6.4ZnO/AlFum MOF), and 64.2% (commercial catalyst). It appears that increasing the loading of Cu on high surface area microporous materials such as MOFs enhances the catalytic activity with respect to CO₂ conversion and methanol productivity due to the high dispersion conferred by the porous support [17,49].

3. Methods and Materials

3.1. Reagents

Aluminum chloride hexahydrate (AlCl₃·6H₂O, Associated Chemical Enterprises, Theta, Johannesburg, South Africa), cupric nitrate trihydrate (Cu(NO₃)₂·3H₂O, Associated Chemical Enterprises, 99.9%, Theta, Johannesburg, South Africa), N,N-dimethyl formamide (DMF, Associated Chemical Enterprises, 99.5%, Johannesburg, Theta, South Africa), sodium hydroxide (NaOH, Associated Chemical Enterprises, Theta, Johannesburg, South Africa), and fumaric acid (C₄H₄O₄, Sigma-Aldrich, 99.9%, Louis, MO, United States) were procured and used directly without any purification. De-ionized water from a water demineralization system, Thermo Fischer Barnstead Smart2Pure, located in the laboratory was used. The commercial catalyst was bought from Alfa Aesar. The pelletized catalyst with a composition of 64.2/24.5/9.8/1.3 wt% (Cu/Zn/Al/Mg) was crushed to a powdery texture prior to usage.

3.2. Synthesis of AlFum MOF

The solvothermal synthesis of AlFum MOF was carried out at ambient pressure. In the procedure, 19.62 g of AlCl₃·6H₂O and 14.76 g of fumaric acid were simultaneously added to 400 mL of DMF in a round-bottom flask. Thereafter, the resultant mixture was stirred at 250 rpm and 130 °C for 4 days. The suspension was then washed twice with acetone and methanol, collected using centrifugation, and dried at 80 °C in an oven. The samples were

activated at 90 °C, under vacuum using a rotary evaporator. Before impregnation with Cu and Zn, the AlFum MOF support was sieved to a size fraction of 50–125 µm.

3.3. Synthesis of AlFum MOF-Supported Catalysts

Cu(NO₃)₂·3H₂O (5.50 mmol) and Zn(NO₃)₂·6H₂O (2.33 mmol) were dissolved using a magnetic stirrer in deionized water (30 mL) in a round-bottom flask. Thereafter, the Cu and Zn-nitrate solution was added slowly to 4.50 g of AlFum MOF whilst stirring continuously. The obtained slurry was continuously mixed at 90 °C, 50 rpm, at ambient pressure for 2 h in a rotary evaporator. Thereafter, the temperature was decreased to 65 °C and the vacuum was activated and maintained for 4 h to furnish a dry, free-flowing powder. The catalyst was labeled 7Cu/3ZnO/AlFum MOF. A similar procedure was followed to produce a catalyst with double the loading of Cu and Zn by mixing Cu(NO₃)₂·3H₂O (9.44 mmol) and Zn(NO₃)₂·6H₂O (4.00 mmol) with AlFum MOF (3.16 g). The catalyst was labeled 15Cu/6.4ZnO/AlFum MOF.

The dried catalyst precursors were heated at 350 °C under a constant flow of argon. The precursors were heated at a rate of 5 °C/min with a hold time of 4 h to furnish catalysts with a theoretical weight percent (wt%) composition of 7/3/90 (7Cu/3ZnO/AlFum MOF) and 15/6.4/78.6 (15Cu/6.4ZnO/AlFum MOF), respectively.

3.4. Characterization

Powder X-ray diffraction (PXRD) was used for crystallinity and the identification of different phases. A Rigaku Ultima IV diffractometer was equipped with Ni-filtered radiation (0.154 nm), 40 kV voltage, and 30 mA current at ambient temperature (Akishimashi, Tokyo, Japan). All analyses were carried out at $2\theta = 3\text{--}90^\circ$ with steps of $0.01^\circ \text{ s}^{-1}$.

The Mettler Toledo, TGA/SDTA 851^e instrument (Mettler Toledo, Greifensee, Switzerland) at a heating rate of $10^\circ \text{C min}^{-1}$ to 900 °C under a constant flow of nitrogen was used for thermogravimetric analysis (TGA). In the analysis, 10 mg of sample was used.

The ASAP 2020 HD analyser (Micromeritics Instrument Corporation, Norcross, GA, USA) was employed to determine the porosity and surface area. The Brunauer-Emmett-Teller (BET) surface areas were measured with nitrogen gas adsorption-desorption isotherms at -196°C and relative partial pressures (p/p_0) of up to 1. Non-linear density functional theory (NLDFT) was used for the estimation of the pore size distributions (PSDs). H-K isotherms were used to determine the pore volumes. Prior to analysis, all samples (>0.2 g) were outgassed under vacuum at temperatures between 150 and 200 °C.

A PerkinElmer Spectrum 100 FTIR spectrometer (PerkinElmer, Waltham, MA, USA) was used for Fourier transform infrared spectroscopy (FTIR) analysis. The spectra were collected at $4000\text{--}550 \text{ cm}^{-1}$.

Helium pycnometry was used to determine the apparent density of the samples. A Micromeritics AccuPyc II 1340 pycnometer (Micromeritics Instrument Corporation, Norcross, GA, USA) was employed with the analysis pressure of helium gas maintained at 135 kPa.

An Auriga Cobra focused-ion beam scanning electron microscope (SEM) coupled with energy-dispersive X-ray spectroscopy (EDS) (Zeiss, Oberkochen, Germany) was used for imaging, elemental mapping, and elemental loading determination in the pristine AlFum MOF and Cu/ZnO/AlFum MOF catalysts. All samples were coated with carbon prior to analysis.

Transmission electron microscope (TEM) imaging was carried out using a JEOL-Jem 2100 model (Joel, Tokyo, Japan), where, prior to analyses, each sample was dispersed in ethanol via ultrasonication for 20 min, transferred to a carbon-coated copper grid, and left to dry overnight. The samples were then mounted onto the stage and analyzed under vacuum.

A Micromeritics Autochem II 2920 analyser (Micromeritics Instrument Corporation, Norcross, GA, USA) was used to determine the reduction profiles of the catalysts via hydrogen temperature-programmed reduction (H₂-TPR). A heating rate of 10°C/min to

150 °C under constant helium flow was used to degas the samples, which were positioned between glass wool in a quartz U-tube. After cooling to 50 °C, each sample was heated at 10 °C/min to 900 °C whilst a constant flow (50 mL/min) of 5% H₂/Ar was maintained. A thermal conductivity detector (TCD) was used to measure the consumption of hydrogen.

X-ray photoelectron spectroscopy (XPS) was used to determine the chemical state of the Cu and Zn active sites. A Thermo Scientific ESCALAB 250Xi instrument (Thermo Fischer Scientific, Kandel, Germany) at 300 W, 100 eV, and X-ray aluminum source at 1486.7 eV was used. All analyses were performed in ultrahigh vacuum of <10⁻⁸ mbar.

3.5. Catalyst Testing

A fixed-bed tubular reactor with dimensions of 27 cm length, internal diameter of 1.01 cm, and external diameter of 1.27 cm was used to evaluate the performance of the catalysts. Each catalyst was sieved to 50–125 µm followed by loading in a catalyst bed with glass wool and placed in the middle of the reactor. After loading in the reactor, the catalysts were reduced with hydrogen at a flow rate of 40 mL/min for 2 h, temperature of 250 °C, and pressure of 20 bar. Subsequently, the temperature of the tubular reactor was decreased to 50 °C, and the gas flow changed to 72% H₂, 24% CO₂, and 4% Ar from a gas bottle mixture. The reactor was then left for 12 h for the gas composition to stabilize. The hydrogenation of CO₂ was performed for 24 h under reactor conditions: temperature = 230 °C; pressure = 50 bar; flow rate = 40 mL/min; and GHSV = 10,000 h⁻¹. An Agilent gas chromatograph instrument: Model 7890B (Agilent Technologies Inc., Santa Clara, CA, USA) was employed for analysis. The hydrocarbons, CH₄ and CH₃OH, were analyzed using a flame ionization detector (FID) and the other gases, CO, CH₄, CO₂, and Ar, were measured with two TCDs. The concentration of the gases was analyzed online and the condensate (CH₃OH and H₂O) was collected in a steel trap immersed in an ice-water bath and analyzed offline. The conversions of CO₂, X, were calculated according to Equation (4):

$$X_{\text{CO}_2} = \left[1 - \left(\frac{\text{CO}_{2, \text{out}}}{\text{CO}_{2, \text{in}}} \right) \times \left(\frac{\text{Ar}_{\text{in}}}{\text{Ar}_{\text{out}}} \right) \right] \times 100 \quad (4)$$

Selectivity to methanol, CO, and CH₄ was calculated using Equations (5)–(7):

$$S_{\text{CH}_3\text{OH}} = \frac{n_{\text{CH}_3\text{OH}}}{n_{\text{CH}_3\text{OH}} + n_{\text{CH}_4} + n_{\text{CO}}} \times 100 \quad (5)$$

$$S_{\text{CO}} = \frac{n_{\text{CO}}}{n_{\text{CH}_3\text{OH}} + n_{\text{CH}_4} + n_{\text{CO}}} \times 100 \quad (6)$$

$$S_{\text{CH}_4} = [1 - (S_{\text{CO}} + S_{\text{CH}_3\text{OH}})] \times 100 \quad (7)$$

where CO₂ (in/out) and Ar (in/out) refer to the initial and outgoing concentrations of CO₂ and Ar, respectively; and S and n refer to the selectivity and moles of each compound, respectively.

4. Conclusions

In this work, Cu-based catalysts supported on AlFum MOF were, for the first time, successfully prepared and evaluated for thermocatalytic hydrogenation of CO₂. The catalyst preparation method resulted in a homogenous, uniform dispersion of Cu and Zn active sites. Doubling the copper loading resulted in a 4-fold increase in CO₂ hydrogenation from 10.8% to 45.6% and an enhancement in methanol productivity. The catalysts exhibited relatively high selectivity toward CO and low selectivity toward methanol when benchmarked with a commercial-grade catalyst. Furthermore, the evaluated catalysts favored the reverse water-gas shift reaction and thereby formed considerable amounts of CO and H₂O under the catalyst testing conditions employed in this study.

Supplementary Materials: The following supporting information can be downloaded at: <https://www.mdpi.com/article/10.3390/catal12101104/s1>, Figure S1: Individual elemental maps of 7Cu/3Zn/AlFum MOF. (a) Al K α 1; (b) Cu K α 1; and (c) Zn K α 1; Figure S2: Individual elemental maps of 15Cu/6.4Zn/AlFum MOF. (a) Al K α 1; (b) Cu K α 1; and (c) Zn K α 1; Figure S3: Derivative TGA plot of AlFum MOF. Figure S4: Derivative TGA plot of 7Cu/3ZnO/AlFum MOF; Figure S5: Derivative TGA plot of 15Cu/6.4ZnO/AlFum MOF.

Author Contributions: Conceptualization, Z.G.D., B.L., K.P. and N.M.M.; methodology, Z.G.D., B.L. and K.P.; investigation, Z.G.D.; resources, N.M.M., H.W.L. and J.M.; writing—original draft preparation, Z.G.D.; writing—review and editing, Z.G.D., H.W.L., J.M., N.M.M. and B.L.; supervision, N.M.M., H.W.L. and J.M.; Formal analysis, Z.G.D.; funding acquisition, N.M.M., B.L. and H.W.L. All authors have read and agreed to the published version of the manuscript.

Funding: This research was funded by Royal Society-Foreign, Commonwealth & Development Office (FCDO) Africa Capacity Building Initiative (ACBI) Programme (Grant AQ150029) and the South African Department of Science and Innovation (DSI) for research activities under HySA Infrastructure (Grant No. CNMH20X).

Data Availability Statement: Not applicable.

Acknowledgments: The authors would like to acknowledge financial support from the Royal Society-Foreign, Commonwealth & Development Office (FCDO) Africa Capacity Building Initiative (ACBI) Programme (Grant AQ150029), the Council for Scientific and Industrial Research (CSIR), and the South African Department of Science and Innovation (DSI) for research activities under HySA Infrastructure (Grant No. CNMH20X) and the South Africa—France PROTEA Programme which is a bilateral incentive programme dedicated to the strengthening of research collaborations between the two countries (Project No. CNMH02X).

Conflicts of Interest: The authors declare no personal and financial conflict of interest.

References

1. Jiang, X.; Nie, X.; Guo, X.; Song, C.; Chen, J.G. Recent Advances in Carbon Dioxide Hydrogenation to Methanol via Heterogeneous Catalysis. *Chem. Rev.* **2020**, *120*, 7984–8034. [[CrossRef](#)] [[PubMed](#)]
2. Tursunov, O.; Kustov, L.; Kustov, A. A Brief Review of Carbon Dioxide Hydrogenation to Methanol Over Copper and Iron Based Catalysts. *Oil Gas Sci. Technol.-Rev. IFP Energ. Nouv.* **2017**, *72*, 30. [[CrossRef](#)]
3. Fischer, H.; Wahlen, M.; Smith, J.; Mastroianni, D.; Deck, B. Ice core records of atmospheric CO₂ around the last three glacial terminations. *Science* **1999**, *283*, 1712–1714. [[CrossRef](#)] [[PubMed](#)]
4. Wang, W.; Wang, S.; Ma, X.; Gong, J. Recent advances in catalytic hydrogenation of carbon dioxide. *Chem. Soc. Rev.* **2011**, *40*, 3703–3727. [[CrossRef](#)]
5. Xiaoding, X.; Moulijn, J.A. Mitigation of CO₂ by Chemical Conversion: Plausible Chemical Reactions and Promising Products. *Energy Fuels* **1996**, *10*, 305–325. [[CrossRef](#)]
6. Bozzano, G.; Manenti, F. Efficient methanol synthesis: Perspectives, technologies and optimization strategies. *Prog. Energy Combust. Sci.* **2016**, *56*, 71–105. [[CrossRef](#)]
7. Ahouari, H.; Soualah, A.; Le Valant, A.; Pinard, L.; Magnoux, P.; Pouilloux, Y. Methanol synthesis from CO₂ hydrogenation over copper based catalysts. *React. Kinet. Mech. Catal.* **2013**, *110*, 131–145. [[CrossRef](#)]
8. Natesakhawat, S.; Lekse, J.W.; Baltrus, J.P.; Ohodnicki, P.R.; Howard, B.H.; Deng, X.; Matranga, C. Active Sites and Structure–Activity Relationships of Copper-Based Catalysts for Carbon Dioxide Hydrogenation to Methanol. *ACS Catal.* **2012**, *2*, 1667–1676. [[CrossRef](#)]
9. Agarwal, A.S.; Rode, E.; Sridhar, N.; Hill, D. Conversion of CO₂ to Value-Added Chemicals: Opportunities and Challenges. In *Handbook of Climate Change Mitigation and Adaptation*; Chen, W.-Y., Suzuki, T., Lackner, M., Eds.; Springer: New York, NY, NY, USA, 2014; pp. 1–40. [[CrossRef](#)]
10. Etim, U.J.; Song, Y.; Zhong, Z. Improving the Cu/ZnO-Based Catalysts for Carbon Dioxide Hydrogenation to Methanol, and the Use of Methanol As a Renewable Energy Storage Media. *Front. Earth Sci.* **2020**, *8*, 545431. [[CrossRef](#)]
11. Qaderi, J. A brief review on the reaction mechanisms of CO₂ hydrogenation into methanol. *Int. J. Innov. Res. Sci. Stud.* **2020**, *3*, 53–63. [[CrossRef](#)]
12. An, X.; Li, J.; Zuo, Y.; Zhang, Q.; Wang, D.; Wang, J. A Cu/Zn/Al/Zr Fibrous Catalyst that is an Improved CO₂ Hydrogenation to Methanol Catalyst. *Catal. Lett.* **2007**, *118*, 264–269. [[CrossRef](#)]
13. Spencer, M.S. The role of zinc oxide in Cu/ZnO catalysts for methanol synthesis and the water-gas shift reaction. *Top. Catal.* **1999**, *8*, 259. [[CrossRef](#)]
14. Dalebout, R.; Visser, N.L.; Pompe, C.E.L.; de Jong, K.P.; de Jongh, P.E. Interplay between carbon dioxide enrichment and zinc oxide promotion of copper catalysts in methanol synthesis. *J. Catal.* **2020**, *392*, 150–158. [[CrossRef](#)]

15. Fisher, I.A.; Bell, A.T. In Situ Infrared Study of Methanol Synthesis from H₂/CO over Cu/SiO₂ and Cu/ZrO₂/SiO₂. *J. Catal.* **1998**, *178*, 153–173. [[CrossRef](#)]
16. Stawowy, M.; Ciesielski, R.; Maniecki, T.; Matus, K.; Łużny, R.; Trawczynski, J.; Silvestre-Albero, J.; Łamacz, A. CO₂ Hydrogenation to Methanol over Ce and Zr Containing UiO-66 and Cu/UiO-66. *Catalysts* **2020**, *10*, 39. [[CrossRef](#)]
17. Rungtaweivoranit, B.; Baek, J.; Araujo, J.R.; Archanjo, B.S.; Choi, K.M.; Yaghi, O.M.; Somorjai, G.A. Copper Nanocrystals Encapsulated in Zr-based Metal-Organic Frameworks for Highly Selective CO₂ Hydrogenation to Methanol. *Nano Lett.* **2016**, *16*, 7645–7649. [[CrossRef](#)] [[PubMed](#)]
18. Jiao, Y.; Liu, Y.; Zhu, G.; Hungerford, J.T.; Bhattacharyya, S.; Lively, R.P.; Sholl, D.S.; Walton, K.S. Heat-Treatment of Defective UiO-66 from Modulated Synthesis: Adsorption and Stability Studies. *J. Phys. Chem. C* **2017**, *121*, 23471–23479. [[CrossRef](#)]
19. Farrusseng, D.; Aguado, S.; Pinel, C. Metal-organic frameworks: Opportunities for catalysis. *Angew. Chem. Int. Ed.* **2009**, *48*, 7502–7513. [[CrossRef](#)]
20. Liang, J.; Liang, Z.; Zou, R.; Zhao, Y. Heterogeneous catalysis in zeolites, mesoporous silica, and metal-organic frameworks. *Adv. Mater.* **2017**, *29*, 1701139. [[CrossRef](#)] [[PubMed](#)]
21. Rambau, K.M.; Musyoka, N.M.; Panek, R.; Franus, W.; Wdowin, M.; Manyala, N. Preparation of coal fly ash derived metal organic frameworks and their carbon derivatives. *Mater. Today Commun.* **2021**, *27*, 102433. [[CrossRef](#)]
22. Gesmanee, S.; Koo-Amornpattana, W. Catalytic hydrogenation of CO₂ for methanol production in fixed-bed reactor using Cu-Zn supported on gamma-Al₂O₃. *Energy Procedia* **2017**, *138*, 739–744. [[CrossRef](#)]
23. Karmakar, S.; Dechnik, J.; Janiak, C.; De, S. Aluminium fumarate metal-organic framework: A super adsorbent for fluoride from water. *J. Hazard Mater.* **2016**, *303*, 10–20. [[CrossRef](#)] [[PubMed](#)]
24. Wang, Y.; Qu, Q.; Liu, G.; Battaglia, V.S.; Zheng, H. Aluminum fumarate-based metal organic frameworks with tremella-like structure as ultrafast and stable anode for lithium-ion batteries. *Nano Energy* **2017**, *39*, 200–210. [[CrossRef](#)]
25. Pan, Y.; Jiang, S.; Xiong, W.; Liu, D.; Li, M.; He, B.; Fan, X.; Luo, D. Supported CuO catalysts on metal-organic framework (Cu-UiO-66) for efficient catalytic wet peroxide oxidation of 4-chlorophenol in wastewater. *Microporous Mesoporous Mater.* **2020**, *291*, 109703. [[CrossRef](#)]
26. Teo, H.W.B.; Chakraborty, A.; Kitagawa, Y.; Kayal, S. Experimental study of isotherms and kinetics for adsorption of water on Aluminium Fumarate. *Int. J. Heat Mass Transf.* **2017**, *114*, 621–627. [[CrossRef](#)]
27. Kobayashi, H.; Taylor, J.M.; Mitsuka, Y.; Ogiwara, N.; Yamamoto, T.; Toriyama, T.; Matsumura, S.; Kitagawa, H. Charge transfer dependence on CO₂ hydrogenation activity to methanol in Cu nanoparticles covered with metal-organic framework systems. *Chem. Sci.* **2019**, *10*, 3289–3294. [[CrossRef](#)]
28. Smyrnioti, M.; Ioannides, T. Dimethyl Ether Hydrolysis over WO₃/γ-Al₂O₃ Supported Catalysts. *Catalysts* **2022**, *12*, 396. [[CrossRef](#)]
29. Felgueiras, M.B.S.; Restivo, J.; Sousa, J.P.S.; Pereira, M.F.R.; Soares, O.S.G.P. Copper Supported on Mesoporous Structured Catalysts for NO Reduction. *Catalysts* **2022**, *12*, 170. [[CrossRef](#)]
30. Alvarez, E.; Guillou, N.; Martineau, C.; Bueken, B.; Van de Voorde, B.; Le Guillouzer, C.; Fabry, P.; Nouar, F.; Taulelle, F.; De Vos, D. The structure of the aluminum fumarate metal-organic framework A520. *Angew. Chem.* **2015**, *127*, 3735–3739. [[CrossRef](#)]
31. Kayal, S.; Chakraborty, A.; Teo, H.W.B. Green synthesis and characterization of aluminium fumarate metal-organic framework for heat transformation applications. *Mater. Lett.* **2018**, *221*, 165–167. [[CrossRef](#)]
32. Jeremias, F.; Fröhlich, D.; Janiak, C.; Henninger, S.K. Advancement of sorption-based heat transformation by a metal coating of highly-stable, hydrophilic aluminium fumarate MOF. *RSC Adv.* **2014**, *4*, 24073–24082. [[CrossRef](#)]
33. Coelho, J.A.; Ribeiro, A.M.; Ferreira, A.F.P.; Lucena, S.M.P.; Rodrigues, A.E.; Azevedo, D.C.S.d. Stability of an Al-Fumarate MOF and Its Potential for CO₂ Capture from Wet Stream. *Ind. Eng. Chem. Res.* **2016**, *55*, 2134–2143. [[CrossRef](#)]
34. Duma, Z.G.; Dyosiba, X.; Moma, J.; Langmi, H.W.; Louis, B.; Parkhomenko, K.; Musyoka, N.M. Thermocatalytic Hydrogenation of CO₂ to Methanol Using Cu-ZnO Bimetallic Catalysts Supported on Metal-Organic Frameworks. *Catalysts* **2022**, *12*, 401. [[CrossRef](#)]
35. Kamyar, N.; Khani, Y.; Amini, M.M.; Bahadoran, F.; Safari, N. Copper-based catalysts over A520-MOF derived aluminum spinels for hydrogen production by methanol steam reforming: The role of spinal support on the performance. *Int. J. Hydrog Energy* **2020**, *45*, 21341–21353. [[CrossRef](#)]
36. Avgouropoulos, G.; Ioannides, T. Effect of synthesis parameters on catalytic properties of CuO-CeO₂. *Appl. Catal. B Environ.* **2006**, *67*, 1–11. [[CrossRef](#)]
37. Djinić, P.; Batista, J.; Levec, J.; Pintar, A. Influence of morphological, redox and surface acidity properties on WGS activity of CuO-CeO₂ catalysts. *J. Chem. Eng. Jpn.* **2009**, *42*, s3–s9. [[CrossRef](#)]
38. Peng, B.; Feng, C.; Liu, S.; Zhang, R. Synthesis of CuO catalyst derived from HKUST-1 temple for the low-temperature NH₃-SCR process. *Catal. Today* **2018**, *314*, 122–128. [[CrossRef](#)]
39. Ye, Q.; Wang, L.; Yang, R.T. Activity, propene poisoning resistance and hydrothermal stability of copper exchanged chabazite-like zeolite catalysts for SCR of NO with ammonia in comparison to Cu/ZSM-5. *Appl. Catal. A Gen.* **2012**, *427–428*, 24–34. [[CrossRef](#)]
40. An, B.; Zhang, J.; Cheng, K.; Ji, P.; Wang, C.; Lin, W. Confinement of Ultrasmall Cu/ZnOx Nanoparticles in Metal-Organic Frameworks for Selective Methanol Synthesis from Catalytic Hydrogenation of CO₂. *J. Am. Chem. Soc.* **2017**, *139*, 3834–3840. [[CrossRef](#)]

41. Farrusseng, D.; Daniel, C.; Hamill, C.; Casaban, J.; Didriksen, T.; Blom, R.; Velte, A.; Fueeldner, G.; Gantenbein, P.; Persdorf, P.; et al. Adsorber heat exchanger using Al-fumarate beads for heat-pump applications—A transport study. *Faraday Discuss.* **2021**, *225*, 384–402. [[CrossRef](#)]
42. Shi, Z.; Tan, Q.; Tian, C.; Pan, Y.; Sun, X.; Zhang, J.; Wu, D. CO₂ hydrogenation to methanol over Cu-In intermetallic catalysts: Effect of reduction temperature. *J. Catal.* **2019**, *379*, 78–89. [[CrossRef](#)]
43. García, A.C.; Moral-Vico, J.; Abo Markeb, A.; Sánchez, A. Conversion of Carbon Dioxide into Methanol Using Cu–Zn Nanostructured Materials as Catalysts. *Nanomaterials* **2022**, *12*, 999. [[CrossRef](#)] [[PubMed](#)]
44. Stangeland, K.; Kalai, D.; Li, H.; Yu, Z. CO₂ Methanation: The Effect of Catalysts and Reaction Conditions. *Energy Procedia* **2017**, *105*, 2022–2027. [[CrossRef](#)]
45. Angelo, L.; Kobl, K.; Tejada, L.M.M.; Zimmermann, Y.; Parkhomenko, K.; Roger, A.-C. Study of CuZnMO_x oxides (M=Al, Zr, Ce, CeZr) for the catalytic hydrogenation of CO₂ into methanol. *Comptes Rendus Chim.* **2015**, *18*, 250–260. [[CrossRef](#)]
46. Joo, O.-S.; Jung, K.-D.; Moon, I.; Rozovskii, A.Y.; Lin, G.I.; Han, S.-H.; Uhm, S.-J. Carbon Dioxide Hydrogenation To Form Methanol via a Reverse-Water-Gas-Shift Reaction (the CAMERE Process). *Ind. Eng. Chem. Res.* **1999**, *38*, 1808–1812. [[CrossRef](#)]
47. Bonura, G.; Cordaro, M.; Cannilla, C.; Arena, F.; Frusteri, F. The changing nature of the active site of Cu-Zn-Zr catalysts for the CO₂ hydrogenation reaction to methanol. *Appl. Catal. B Environ.* **2014**, *152–153*, 152–161. [[CrossRef](#)]
48. Gaab, M.; Trukhan, N.; Maurer, S.; Gummaraju, R.; Müller, U. The progression of Al-based metal-organic frameworks—From academic research to industrial production and applications. *Microporous Mesoporous Mater.* **2012**, *157*, 131–136. [[CrossRef](#)]
49. Joo, S.H.; Park, J.Y.; Tsung, C.-K.; Yamada, Y.; Yang, P.; Somorjai, G.A. Thermally stable Pt/mesoporous silica core-shell nanocatalysts for high-temperature reactions. *Nat. Mater.* **2009**, *8*, 126–131. [[CrossRef](#)]